

See discussions, stats, and author profiles for this publication at: <https://www.researchgate.net/publication/5352374>

Cutting Edge Structural Protein from the Jaws of *Nereis virens*

ARTICLE *in* BIOMACROMOLECULES · JULY 2008

Impact Factor: 5.75 · DOI: 10.1021/bm800200a · Source: PubMed

CITATIONS

10

READS

48

4 AUTHORS, INCLUDING:



[Tom Laue](#)

University of New Hampshire

140 PUBLICATIONS 4,458 CITATIONS

[SEE PROFILE](#)

Cutting Edge Structural Protein from the Jaws of *Nereis virens*

Chris C. Broomell,*† Sue F. Chase,‡ Tom Laue,‡ and J. Herbert Waite†

University of California at Santa Barbara, Santa Barbara, California 93106, and Center to Advance Molecular Interaction Science, University of New Hampshire, Durham, New Hampshire 03824

Received February 21, 2008; Revised Manuscript Received April 7, 2008

The fang-like jaws of the marine polychaete *Nereis virens* possess remarkable mechanical properties considering their high protein content and lack of mineralization. Hardness and stiffness properties in the jaw tip are comparable to human dentin and are achieved by extensive coordination of Zn²⁺ by a histidine-rich protein framework. In the present study, the predominant protein in the jaw tip, Nvjp-1, was purified and characterized by partial peptide mapping and molecular cloning of a partial cDNA from a jaw pulp library. The deduced amino acid sequence revealed an ~38 kDa histidine-rich protein rich in glycine and histidine (~36 and 27%, respectively) with no well-defined repetitive motifs. The effects of pH and metal treatment on aggregation, secondary structure, and hydrodynamic properties of recombinant Nvjp-1 are described. Notably, Zn treatment induced the formation of amyloid-like fibers.

Introduction

The combination of lightweight construction and robust mechanical properties of invertebrate biting and piercing structures underscores their potential as models for improved synthetic materials. Mechanical properties in these structures exceed those of synthetic polymers and are often comparable to highly mineralized tissues from higher organisms.^{1–4} In stark contrast to mineralized tissues, however, the structural framework of sclerotized “tools” from invertebrates is predominantly organic. Most consist of highly ordered composites of carbohydrate, protein, and polyphenolic compounds, with significant variation in architecture and relative compositions between organisms.^{5–7} The development of novel materials with similar attributes will require a fundamental understanding of the relationship between composition, architecture, and mechanical properties in the parent structures. Significant progress has been made toward the mechanical and structural characterization for several materials, including some jaws and mandibles.^{1,2,4,6,8–10} However, relatively little is known about the organic components, particularly the structural proteins that make up the scaffolding framework.

We have previously described the relationship between metal content and mechanical properties in the jaws of *Nereis virens*, a burrowing polychaete common to the North Atlantic region.^{1,3} The jaws are the worm’s primary tools for feeding and defense and, as such, must be optimized for grasping, piercing, and tearing prey in an abrasive environment. Hardness and stiffness properties in the jaw are comparable to human dentin and superior to synthetic polymers. Amino acid analysis indicates that the jaws are composed of roughly 90% (w/w) protein, with a strong compositional bias toward glycine and histidine.^{3,11} The remainder of the jaw is comprised of halogens (~8%) and Zn ions (~2%).^{12,13}

In undertaking this investigation, we hypothesized the cutting edge of the *Nereis* jaw (i.e., the tip and serrated distal end) to be composed chiefly of histidine-rich Zn binding proteins. We

describe the purification of Nvjp-1, a protein from the distal jaw that contains over 25 mol % histidine. We also describe the effects of pH and zinc treatment on aggregation, secondary structure, and hydrodynamic properties of recombinant Nvjp-1.

Materials and Methods

Nvjp-1 Purification. Live worms (*Nereis virens* Sars) were purchased from Harbor Bait (Wiscasset, ME, USA) and frozen at –80 °C upon receipt. Jaws were dissected from fresh-thawed worms, air-dried, and pulverized under liquid nitrogen with a ceramic mortar and pestle. Protein was extracted by homogenizing jaw powder in 5% acetic acid/8 M urea with protease inhibitors (leupeptin and pepstatin, each at 1 mg/mL). Homogenates were clarified by centrifugation at 10000 × g for 30 min at 4 °C. Urea was removed from extract supernatant by ultrafiltration with an Amicon Ultra-4 filtration column (10 kDa MWCO) (Millipore, MA). Jaw powders were cleaned (post extraction) by extensive washing with Milli-Q water. Nvjp-1 was purified from jaw extracts by successive rounds of cation exchange FPLC and C-8 RP-HPLC as follows. Extracts were applied to a HiTrap SP-XL column (GE Healthcare Biosciences, NJ, USA), pre-equilibrated with 50 mM sodium acetate (pH 5) and eluted with a gradient of 0–2 M guanidinium HCl in 50 mM sodium acetate (pH 5) over 60 min. Fractions containing histidine-rich proteins (see below) were pooled and concentrated and loaded onto a Brownlee Aquapore RP-300 C8 column (7 μm) pre-equilibrated with 10% acetonitrile/0.1% trifluoroacetic acid (TFA). Proteins were eluted in a gradient of 10–100% acetonitrile in 0.1% TFA over 60 min. Fractions were lyophilized and reconstituted in Milli-Q water. SDS and acid urea (AU) PAGE were carried out as described elsewhere.^{14–16} Coomassie Blue was used to stain total protein. Histidine-rich and red-ox active proteins were identified using Pauly’s stain and nitrobluetetrazolium (NBT), respectively, as described elsewhere.^{17,18}

Peptide Generation and Sequencing. Nvjp-1 was treated with *S. aureus* V8 protease (Glu-C endopeptidase) in 50 mM sodium phosphate (pH 5.8) in sealed vessels for 24 h at 25 °C. Under these conditions proteolysis occurs following Glu and Asp residues.¹⁹ Peptides were purified on a Phenomenex Jupiter C18 column (5 μm) with a gradient of acetonitrile (5–100% in 0.1% TFA over 60 min), lyophilized, and reconstituted in Milli-Q water prior to analysis by either Edman or electrospray ionization tandem mass spectrometry (ESI-MS/MS) sequencing. Edman sequencing was performed as described elsewhere.²⁰

* To whom correspondence should be addressed. Email: broome@lifesci.ucsb.edu.

† UC at Santa Barbara.

‡ University of New Hampshire.

ESI-MS/MS was performed on a Micromass QTOF2 tandem mass spectrometer (Waters Corporation, MA) with an electrospray ionization source. Samples were infused by syringe pump into the ESI source at 5 $\mu\text{L}/\text{min}$. Analysis parameters were as follows: capillary potential 3.5 KV, skimmer cone voltage 40 V, mass range 100–2000 m/z , data collection rate of 1 scan/sec with 0.1 s between scans. Argon was used as collision gas at a voltage of 25 V.

Amino Acid Composition Analysis. Samples were hydrolyzed in vacuo at 110 °C in 6 M HCl supplemented with 10 μL phenol. Following hydrolysis (24 and 72 h for liquid and solid samples, respectively) samples were washed extensively in Milli-Q water and methanol. Amino acid compositions were determined on a Beckman Coulter 63000 Amino Acid Analyzer using ninhydrin-based postcolumn derivatization as previously described.²⁰

Molecular Cloning. RNA was isolated from the jaw-associated pulp tissue of freshly sacrificed worms by Trizol (Invitrogen, CA) extraction according to the manufacturer's instructions. Approximately 100 μg of total RNA was used to generate double strand cDNA. A cDNA library was made using the CloneMiner cDNA Library Construction Kit (Invitrogen, U.S.A.) according to the manufacturer's instructions. Nvjp-1 clones were identified by PCR using degenerate oligonucleotide primers designed from peptide sequences. Additional sequence was obtained via 5' and 3' RACE using both BD Smart (Clonetec, CA) and GeneRacer (Invitrogen) kits with nondegenerate primers designed from initial screening trials.

Recombinant Nvjp-1/Protein Expression. A recombinant construct for Nvjp-1 (rNvjp-1) was amplified from *Nereis* jaw pulp cDNA using the following oligonucleotide primers: (5') GGATTCCACAAAGATG-GTTATGGACATGATGAT and (3') GAATTCTGTTCAAGTAACTAAT-GATG (adding BamHI and EcoRI restriction sites to the 5' and 3' ends, respectively). Constructs were cloned into the pGEM-Teasy vector (Promega, Madison, WI) for maintenance in TOP10 *E. coli* (Invitrogen, Carlsbad, CA) and subcloned into the pET28a vector (Invitrogen) for expression in BL23-DE3 cells according to the manufacturer's instructions. Bacteria were lysed by French press in 50 mM sodium phosphate/6 M guanidinium chloride (pH 7.4). Lysate supernatants were applied to a hi-trap metal chelating column (Amersham) charged with ZnCl₂. Bound protein was eluted with an imidazole gradient (0–200 mM over 15 min), desalting by reverse phase C8 HPLC, lyophilized, and reconstituted in Milli-Q water prior to further analyses. Amino acid composition analysis was used to confirm the identity of the purified product and for protein quantification. Note that the pET28a vector encodes a short N-terminal peptide sequence which includes a His₆-tag and a thrombin cleavage site. Initial solubility and fibrillization tests did not reveal any differences between intact rNvjp-1 and rNvjp-1 following thrombin treatment and purification. Therefore, intact rNvjp-1 was used in all subsequent experiments.

Nvjp-1 Solubility. Aliquots of rNvjp-1 (20 μM in Milli-Q water) were mixed with an equal volume of the appropriate buffer and incubated for 12 h at 25 °C. Above pH 7, a flocculent precipitate formed immediately following pH adjustment but cleared within 3 h. For metal-treated samples, ZnCl₂ was added to rNvjp-1 prior to mixing with buffer (final Zn/protein ratio = 20). Following incubation, samples were centrifuged for 30 min at 17000 $\times g$ and the supernatant collected for further analysis. The soluble fraction was determined by normalizing the absorbance at 280 nm of each sample to that of centrifuged, unbuffered rNvjp-1. Solubility was tested in 50 mM sodium phosphate (pH 4.5–9.5), 20 mM HEPES (pH 6.0–8.0), and Tris acetate (pH 5.0–9.0). For ZnCl₂ studies, solubility was measured in 20 mM HEPES \pm 100 mM NaCl (pH 8).

ATR-FTIR Spectroscopy. IR spectra were collected on Nicolet Magna 850 infrared spectrometer in 50 mM sodium phosphate/100 mM NaCl buffer prepared with deuterium oxide (final protein concentration = 0.5 mg/mL). Data were collected using an attenuated total reflectance (ATR) device equipped with a ZnSe crystal. A total of 128 scans were taken at a resolution or 4 cm^{-1} . Fourier self-deconvolution was applied to increase spectral resolution in the amide I' region (1600–1700 cm^{-1})

as described by Byler et al.²¹ Origin software (OriginLab Corporation, Northampton, MA) was used to quantify structural components using a least-squares curve fitting assuming Gaussian peak shapes with peak centers determined from second derivative spectra.

Analytical Ultracentrifugation. Sedimentation velocity studies were carried out in a Beckman model XL-A analytical ultracentrifuge using absorbance optics at 230 nm. The buffer conditions were 10 mM Tris acetate, 100 mM NaCl at pH 5.5 and 8. Initial runs were conducted at 3000 rpm to resolve high molecular mass aggregates. Extended runs were performed at 45000 rpm (pH 8) and 60000 rpm (pH 5.5) at 20 °C. Sedimentation coefficients were calculated in SEDFIT either by (i) assuming a single weight average frictional coefficient (f/f_o) for all species (i.e., c(s) distribution) or by (ii) assuming a two-dimensional distribution of sedimentation and frictional coefficients (i.e., c(s, f/f_o)).^{22,23} Buffer density and viscosity were fixed at 1.005 g/cm³ and 0.0102 Poise, respectively. Based on the amino acid sequence, the partial specific volume of rNvjp-1 was estimated to be 0.728 cm³/g. For c(s) calculations, the frictional ratio was allowed to float. Confidence levels used were 95%.

Atomic Force Microscopy. rNvjp-1 (20 μM in Milli-Q water) was diluted 1:2 with the appropriate buffer and incubated for 3 h at room temperature. A small aliquot was spotted onto a freshly cleaved mica disk and allowed to incubate for ~30 s prior to rinsing by immersion in Milli-Q water. Samples were partially dried under a gentle stream of nitrogen. For metal treated samples, rNvjp-1 was mixed with 0.1 volume ZnCl₂ solution to yield final Zn/protein ratios of 1, 5, 10, and 20 prior to buffer addition. Samples were imaged using a Multimode AFM with a Nanoscope V controller (Veeco Metrology, Inc., Santa Barbara, CA). All images were collected under ambient conditions in tapping mode using OTESPA silicon nitride cantilevers.

Results

Figure 1A depicts a worm with its proboscis extended and jaws exposed. Amino acid composition of intact *Nereis* jaws is dominated by relatively few residues, with significant contributions from glycine and histidine.^{3,12} As demonstrated previously and summarized here, amino acid distribution is asymmetric in the jaw. This is most apparent with histidine and alanine, which exhibit opposing gradients from tip to base. (Figure 1B) The variance in amino acid distribution suggests that (i) *Nereis* jaws are composed of at least two compositionally distinct proteins and (ii) the histidine-rich component is more abundant in the jaw tip.

To further characterize the composition of structural proteins in the jaw, pooled jaws ($n = 1000$) were pulverized and extracted with 5% (v/v) acetic acid/8 M urea. Less than 20% the jaw mass was extractable (even with repeated extractions). Table 1 compares amino acid compositions of bulk jaw powder before and after protein extraction. Compositions were also determined for jaws ($n = 100$) that had been sectioned into tips and bases prior to pulverization. Overall, values for most residues were similar between soluble and insoluble fractions, suggesting that compositions were comparable. Surprisingly, histidine levels were reduced in the insoluble fractions of whole jaws and, to a lesser extent, in the jaw tips. The implications of this observation are discussed below.

Nereis jaw extracts were analyzed by acid urea (AU) and SDS-PAGE. Coomassie staining revealed multiple proteins in jaw extracts with one major component, referred to here as Nvjp-1 (*N. virens* jaw protein-1; Figure 1D, lane 1). Although Nvjp-1 was present globally, it was significantly enriched in tip extracts where it was the predominant component (lanes 2 and 3). Staining of separate gels with Pauly and NBT stains (Figure 1D, lanes 4 and 5, respectively) indicated that Nvjp-1 is both histidine-rich and mildly redox active. The nature of

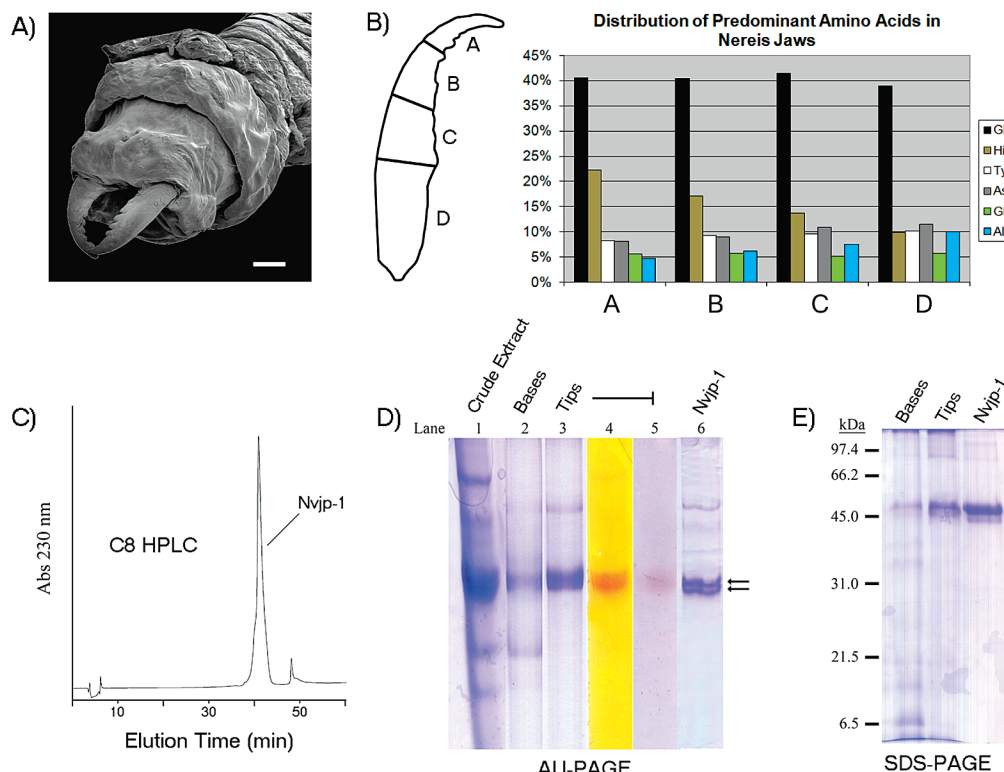


Figure 1. Amino acid composition and distribution in *Nereis* jaws. (A) Electron micrograph showing a typical specimen with proboscis extended and jaws exposed (scale bar 1 mm). (B) Distribution of the major amino acid residues in the jaw. Jaws were sectioned as indicated prior to hydrolysis. (C) C8 HPLC of histidine-rich fractions from cation exchange FPLC. (D) Gel electrophoresis (AU-PAGE) comparing whole jaw, tip, and base extracts (lanes 1–5) with purified Nvjp-1 (lane 6). Arrows to the right of lane 6 indicate that Nvjp-1 migrates as two bands under acid urea conditions. Pauly staining and NBT (lanes 4 and 5, respectively) demonstrate that the major protein component in the tip is histidine-rich and mildly redox active. (E) Gel electrophoresis (SDS-PAGE) comparing tip and base extracts with purified Nvjp-1.

redox cycling in Nvjp-1 is not known, however, trace levels of 3,4-dihydroxyphenylalanine (DOPA) have been detected in intact jaws (unpublished data) and jaw hydrolysates.¹²

Nvjp-1 was purified from jaw extracts by successive rounds of cation exchange FPLC and C8 RP-HPLC. Pauly staining was used to select FPLC fractions containing Nvjp-1 (not shown), which were pooled and concentrated prior to HPLC (Figure 1C). The amino acid composition of purified Nvjp-1 matched closely that of the insoluble material from the jaw tip (Table 1), although histidine content was notably higher in the purified protein. Nvjp-1 migrated as two bands of equal intensity on AU gels (Figure 1D, lane 6, indicated by arrows), indicating either two low-pH charge states of Nvjp-1 or, alternatively, two distinct protein components with similar charges. Two components were also discernible on SDS gels (~50 and ~45 kDa), however, only the larger component appeared to be present in significant quantity (Figure 1E). Both bands were enriched in jaw tips and stained positive with Pauly stain (not shown). MALDI-TOF spectra of Nvjp-1 also revealed two components, major and minor, with *m/z* of ~38 and ~35 kDa, respectively (not shown). Disagreements between molecular weights as determined by SDS-PAGE and MALDI-TOF analyses are interesting but not surprising given the entirely empirical basis of SDS-PAGE.

A *Nereis* jaw pulp cDNA library was screened with PCR using primers based on sequences of peptides purified from Nvjp-1 digests. A degenerate primer for the sequence *HHQLDGYEKD*, in conjunction with a vector specific primer, successfully amplified a sequence corresponding to the C-terminus of Nvjp-1 (including the 3' untranslated region and poly A tail). Additional sequence was obtained by means of a 5' RACE strategy with nondegenerate primers to sequences obtained from the first round of screening.

The partial cDNA and deduced amino acid sequences of Nvjp-1 are presented in Figure 2. Underlined residues indicate sequences that were later confirmed by Edman and/or ESI-MS/MS sequencing of additional peptides from purified Nvjp-1. Two major size variants of Nvjp-1 were consistently detected in all cDNA preparations, consisting of the larger *Nvjp-1a* and a potential truncation product, *Nvjp-1b*. Alignment of sequences from all clones revealed an additional variant similar to *Nvjp-1a* (hereafter termed “*Nvjp-1a₁* and *Nvjp-1a₂*”), which consisted of the deletion of two *GH* repeats (residues 40–43) and an insertion of one additional *GYGGHG* repeat (residues 83–88, based on the sequence of *Nvjp-1a₁*). The combined frequencies of *Nvjp-1a₁*, *Nvjp-1b*, and *Nvjp-1a₂* from all cDNA preparations were 0.56, 0.33, and 0.11, respectively. The predicted amino acid compositions of all variants were nearly identical to each other (not shown) and to that of purified Nvjp-1 (Table 1, predicted cDNA sequence represents *Nvjp-1a₁*). The range of predicted molecular weights of all three variants spans from ~32 to ~40 kDa. This is close to the observed mass of purified Nvjp-1 (~35 to ~38 kDa). It does suggest, however, that additional processing (e.g., post-translational additions and/or cleavage) is involved in Nvjp-1 maturation.

In theory, Edman sequencing should provide insight into any variants in protein preparations (i.e., residues from the N-termini of all components would be represented in Edman sequences of purified Nvjp-1). However, no sequence was obtainable from the intact Nvjp-1 preparation, suggesting that the termini might be blocked. We were also unable to obtain any unambiguous sequence information from peptides generated from the N-terminal half-of Nvjp-1. Most peptides could not be resolved by HPLC, presumably due to similarities in composition and size (as predicted from the cDNA sequence). Several mixed

Table 1. Comparison of the Amino Acid Compositions of Whole Jaws (i) with the Nonextractable Fraction from (ii) Intact and (iii, iv) Sectioned Jaws with that of Nvjp-1 (v) as Purified and (vi) Predicted from its cDNA^a

residue	whole jaw hydrolysate (i)	jaw solids—unextractable fraction				Nvjp-1 (predicted; vi)
		whole jaw (ii)	bases (iii)	tips (iv)	Nvjp-1 (purified; v)	
Asx	9.08	10.17	9.49	9.08	9.30	9.14
Thr	1.13	0.84	1.34	1.14	0.93	1.04
Ser	2.59	0.91	2.56	2.55	2.60	3.13
Glx	4.57	5.65	5.85	6.07	6.79	6.53
Pro	0.00	0.74	2.26	1.98	0.25	0.52
Gly	35.09	39.16	36.47	35.87	36.66	36.29
Ala	7.83	7.84	9.77	5.73	3.74	2.09
Val	1.23	1.52	3.81	1.55	1.38	0.52
Ile	0.66	0.84	1.35	1.25	0.24	0.52
Leu	1.24	1.12	1.34	1.06	1.71	0.52
Tyr	9.65	9.67	10.21	8.35	5.75	7.31
Phe	1.81	1.68	1.79	1.65	1.72	1.83
His	21.68	15.64	10.78	19.24	26.00	26.64
Lys	1.45	2.18	1.36	2.19	2.10	2.35
Arg	1.99	2.05	1.62	2.29	0.83	1.57
Total	100%	100%	100%	100%	100%	100%

^a The close agreement between the profiles of tip residue and Nvjp-1 strongly suggest that it dominates the composition in the distal jaw. All numbers represent the mol % amino acid in sample hydrolysates. Standard deviations are approximately 10%.

Nvjp-1a1 HNDGYGHDDHHGHGHGGYGGHGDYGGHGHGGYGGHGHGHGHFDDHPFYTI PAFG 60

Nvjp-1a2 HNDGYGHDDHHGHGHGGYGGHGDYGGHGHGGY--- GHGHGHGHFDDHPFYTI PAFG 56

Nvjp-1b G 1 *

Nvjp-1a1 HGYGHGHHGGHGHGGYGGHDYGGHGGYGGYGGY--- DHGHGGHGYGSHGGHGQDYGG 114

Nvjp-1a2 HGHGHHGGHGHGGYGGHDYGGHGGYGGHGGYGDHGHHGGHGYGSHGGHGQDYGG 116

Nvjp-1b HGYGHGHHGGHGHGGYGGHDYGGHGGYGGHGGYGGY--- DHGHGGHGYGSHGGHGQDYGG 55

*** : ***** : ***** : ***** : ***** : ***** : *****

Nvjp-1a1 DYGGHGHHHHGGHDHDDFGHDFGHGGDHGHGGHHGHHDGYGHQDQGHGHGHGDYDY 174

Nvjp-1a2 DYGGHGHHHHGGHDHDDFGHDFGHGGDHGHGGHHGDYGHQDQGHGHGDYDY 176

Nvjp-1b DYGGHGHHHHGGHDHDDFGHDFGHGGDHGHGGHHGDYGHQDQGHGHGDYDY 115

***** : ***** : ***** : ***** : ***** : ***** : *****

Nvjp-1a1 SH**GNQHDNGHREHYGGHQAAAGHHGHEGSGSHYGGQGGGGSHHSGGHDGSHNHGKFQTQY** 234

Nvjp-1a2 GHGNQHDNGHREHYGGHQAAAGHHGHEGSGSHYGGQGGGGSHHSGGHDGSHNHGKFQTQY 236

Nvjp-1b SHGNQHDNGHREHYGGHQAAAGHHGHEGSGSNHGQGGGGSHHSGGHDGSHNHGKFQTQY 175

.***** : ***** : ***** : ***** : ***** : *****

Nvjp-1a1 **SYRGNDKYGGHNQYQGHGAYNEY**SKSKGTGKYVAHGTTEEGHHQLDGYEKDNHQGKYEGHG 294

Nvjp-1a2 SYRGNDKYGGHNQYQGHGAYNEYSKSKGTGKYVAHGTTEEGHHQLDGYEKDNHQGKYEGHG 296

Nvjp-1b SYRGNDKYGGHNQYQGHGAYNEYSKSKGTGKYVAHGTTEEGHHQLDGYEKDNHQGKYEGHG 235

***** : ***** : ***** : ***** : *****

Nvjp-1a1 EHHSHQHGDKHHKRKEHDHAGIS**GFHGQGHVQGNHALHGHGGGGHGHGEHGSARGH** 354

Nvjp-1a2 EHHSHQHGDKHHKRKEHDHAGISGFHGQGHVQGNHALHGHGGGGHGHGEHGSARGH 356

Nvjp-1b EHHSHQHGDKHHKRKEHDHAGISGFHGQGHVQGNHALHGHGGGGHGHGEHGSARGH 295

***** : ***** : ***** : ***** : *****

Nvjp-1a1 **HGGGGYGGGGHGRGHGGHQGHGHH** 381

Nvjp-1a2 HGGGGYGGGGHGRGHGGHQGHGHH 383

Nvjp-1b HGGGGYGGGGHGRGHGGHQGHGHH 319

Figure 2. Deduced amino acid sequences of Nvjp-1 variants recovered from screening of Nereid jaw pulp cDNA. Asterisks represent conserved residues. Underlined sequences in Nvjp-1a1 were directly identified in peptides purified from Glu-C protease digests of Nvjp-1 (Edman and ESI-MS/MS sequencing). Confirmation of italicized residues is inferred from mass fingerprint analysis of peptide digests in conjunction with peptide sequencing.

sequences were obtained that were high in Gly, His, and, notably, Asp residues (i.e., multiple peaks were present in each sequencing cycle). Based on the sequence predicted from the cDNA, such compositions are more likely to result from N-terminal peptides. Over 80% of the Asp occurs in this region, and all Asp-containing regions from the C-terminus were successfully identified in other peptides.

The solubility of rNvjp1 was assessed as a function of pH and ZnC₂ treatment. Both factors have been shown to effect

structural transitions and the associated supramolecular assembly of various fiber-forming proteins and peptides. It is notable that rNvjp1 exhibited rather low solubility even under optimal conditions. Only ~45% of the total protein remained in supernatants of extreme low and high pH samples following extensive centrifugation (Figure 3A, diamonds). Similar aggregation profiles were observed with alternative buffers, notably sodium and Tris-acetate between pH 5.0 and 9.0 and HEPES between 6.0 and 8.0 (not shown). The solubility of rNvjp1 was

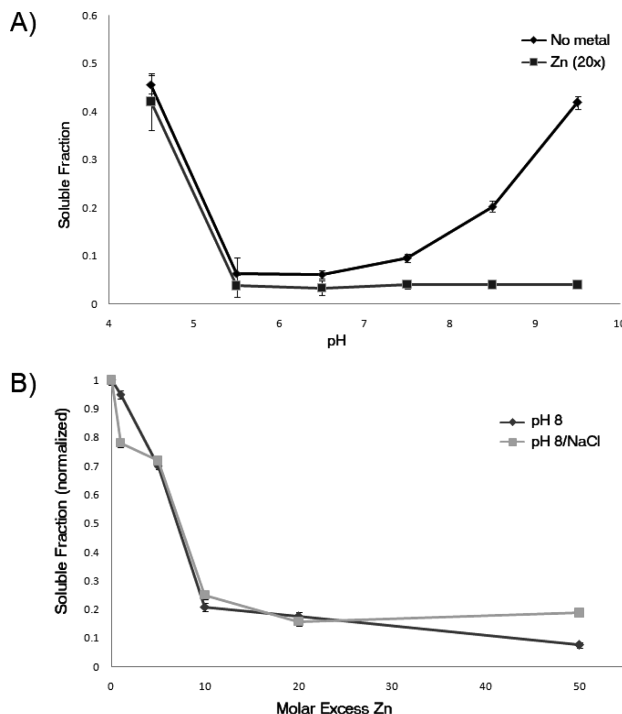


Figure 3. Nvjp-1 solubility. (A) Nvjp-1 solubility is explored as a function of pH, from 4.5–9.5 in phosphate buffer without (diamonds) and with (squares) a 20-fold molar excess of ZnCl_2 . (B) Nvjp-1 solubility as a function of ZnCl_2 ratio. Solubility was determined at pH 8 with (squares) and without (diamonds) 100 mM NaCl.

minimal between pH 6 and 6.5, consistent with its calculated isoelectric point ($\text{pI} = 6.5$). Addition of a 20-fold molar excess of Zn^{2+} had no apparent effect on solubility at low pH (Figure 3A, squares). However, above pH 6.5, Zn^{2+} treatment resulted in a complete and irrecoverable loss of rNvjp1 from solution. Figure 3B shows the effects of increasing Zn ion concentrations on rNvjp-1 solubility at pH 8.0. Zn^{2+} induced significant rNvjp-1 aggregation even at low levels; about 80% of the protein was precipitated at a $\text{Zn}/\text{protein}$ molar ratio of 10 and aggregation was only slightly increased at a $\text{Zn}/\text{protein}$ ratio of 50 (Figure 3B, diamonds). As salt concentration has been shown to influence aggregation of various amyloidogenic proteins,^{24–27} we also examined rNvjp-1 solubility in HEPES buffer containing 100 mM NaCl. For both buffers, no significant differences in protein aggregation were observed at $\text{Zn}/\text{protein}$ ratios ≥ 5 (Figure 3B, squares). However, rNjp-1 aggregation was slightly increased at a $\text{Zn}/\text{protein}$ ratio of 1 in buffer with NaCl.

Atomic force microscopy was used to examine the morphologies of rNvjp-1 oligomers formed under various conditions (Figure 4). Although most aggregates formed without Zn^{2+} were amorphous, there were some differences between those formed with and without NaCl. In the absence of NaCl, protein aggregates were ≤ 1 nm in height with a slightly diffuse appearance and were broadly dispersed on the mica without any obvious clustering (Figure 4A). Aggregates formed in HEPES/NaCl were generally on the order of 3–6 nm in height with more sharply defined edges and were frequently absorbed in clusters or semicontinuous networks (Figure 4C). Treatment with ZnCl_2 dramatically altered the characteristics of rNvjp-1 aggregates. At $\text{Zn}/\text{protein} \approx 1$, oligomers were no longer deposited in disperse fields but, instead, consisted of either spheroidal or slightly elongated structures in HEPES (Figure 4B) or, notably, extended fibers in HEPES/NaCl (Figure 4D). Similar shapes were observed at $\text{Zn}/\text{protein} \approx 5$; at higher

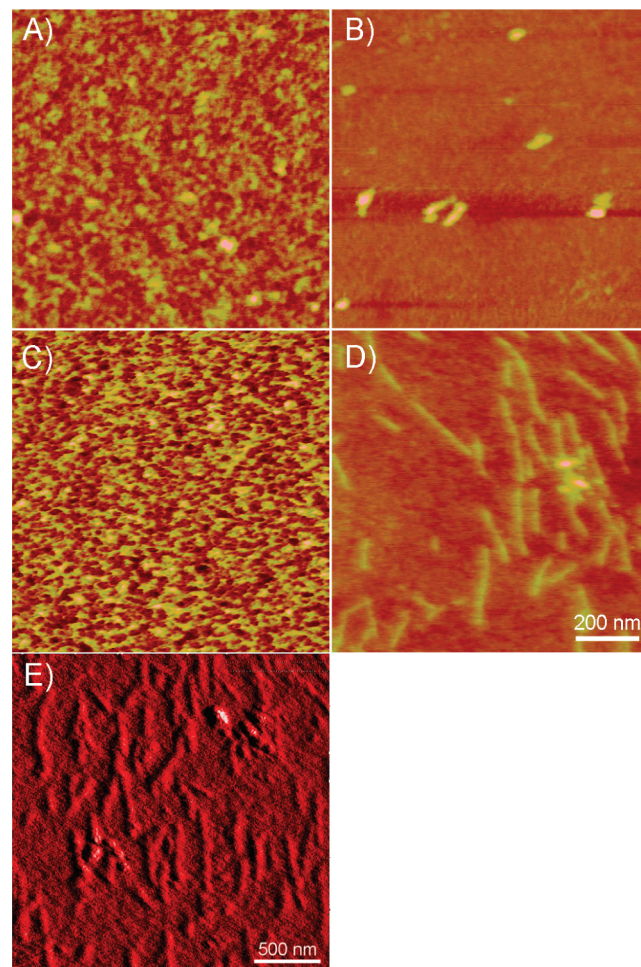


Figure 4. Atomic force microscopy. (A–D) Height images of rNvjp-1 aggregates formed at pH 8 in (A) HEPES, (B) HEPES with ZnCl_2 ($\text{Zn}/\text{protein} \approx 1$), (C) HEPES/NaCl, and (D) HEPES/NaCl with ZnCl_2 ($\text{Zn}/\text{protein} \approx 1$). (E) Image (amplitude channel) of larger fibers also observed in HEPES/NaCl with ZnCl_2 .

ratios, all aggregates were amorphous (not shown). In HEPES, oligomers were approximately 4–5 nm high and 25–30 nm wide (width at half-height). Lengths of elongated species ranged from 60–80 nm. Some longer filaments (e.g., ≥ 100 nm) were observed without NaCl, although they were infrequent and not reproducible (not shown). Fibers formed in HEPES/NaCl were generally 200–300 nm in length with heights and widths of ~ 1.5 and ~ 25 nm, respectively. A few longer fibers (500–800 nm) were also observed (Figure 4E). Longer fibers were also generally wider (~ 50 –60 nm) and occasionally appeared to form helical or twisted structures.

Figure 5 shows FTIR spectra for the amide I' region of rNvjp-1 in deuterated phosphate-buffered saline. Prominent peaks at pD 5.5 were at 1645 cm^{-1} ($\sim 40\%$), 1661 cm^{-1} ($\sim 22\%$), and 1675 cm^{-1} ($\sim 22\%$). Bands at 1645 cm^{-1} and 1675 cm^{-1} are generally assigned to random coil and turns/loops, respectively.^{21,28–31} Peaks at 1661 cm^{-1} have been associated with both α -helices and extended turns.^{21,30} Smaller peaks associated with beta structure were observed at 1631 cm^{-1} and 1691 cm^{-1} ($\sim 16\%$ total).^{21,30} Significant differences in the amide I' peak were observed in the pD 8 samples, notably, the complete loss of the random coil component (1645 cm^{-1}), a slight increase in the band at 1675 cm^{-1} ($\sim 27\%$), and the appearance of bands at 1615 cm^{-1} , 1625 cm^{-1} , and 1696 cm^{-1} ($\sim 7\%$ total; Figure 5B). These latter features are typically associated with β -sheet. Additionally, the 1661 cm^{-1} band

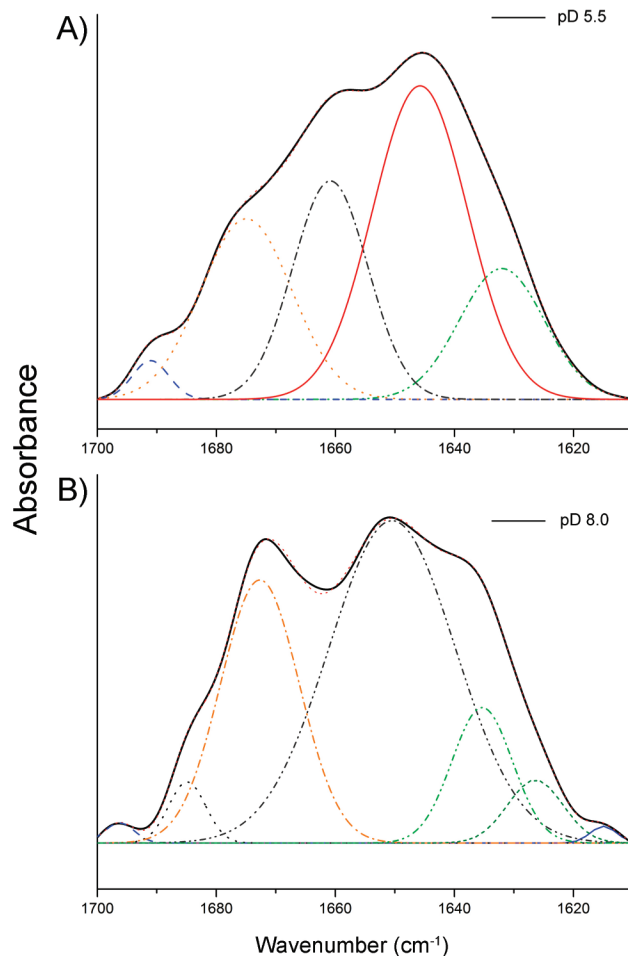


Figure 5. ATR-FTIR of rNvjp-1. Amide I' regions of rNvjp-1 in deuterated 50 mM sodium phosphate/100 mM NaCl at (A) pD 5.5 and (B) pD 8. The components of each amide I' peak were determined by deconvolution using peak centers determined from second derivative spectra. The resulting spectra calculated for the deconvoluted peaks are represented by dotted red lines (these essentially overlap with the experimental spectra; $r^2 > 0.999$ for each sample).

exhibited a frequency shift to 1651 cm^{-1} and increased in intensity ($\sim 53\%$). A slight shift was also observed for the high frequency β -sheet feature at 1685 cm^{-1} .

The effect of pH on hydrodynamic properties of rNvjp-1 was probed by analytical ultracentrifugation. The major rNvjp-1 species in solution at pH 5.5 was monomeric with a sedimentation coefficient of $\sim 2.3\text{ S}$ (Figure 6A, top). A small amount of larger material ($\sim 4\text{ S}$) was detected as well as an additional slower-sedimenting species at $\sim 1.4\text{ s}$. At pH 8, over 80% of the protein sedimented within 5 min at 3000 rpm (not shown), indicating that most of the protein was associated with high order oligomers ($> 10000\text{ S}$). The sedimentation profile for the remaining protein indicated multiple species with sedimentation coefficients ranging from $\sim 0.5\text{--}3\text{ S}$, with a major component at 1.4 S (Figure 6A, middle). This trend toward lower sedimentation coefficients suggested either (i) significant fragmentation of rNvjp-1 at high pH or (ii) high pH induced a significant change in molecular shape, notably a trend toward higher axial ratios (Figure 7). No fragmentation of rNvjp-1 was indicated by SDS-PAGE or ESI-mass spectrometry (Figure 6B,C). The pH 8 data were also fit using an alternative sedimentation model which allows for nonuniform distributions in molecular shape. This model predicted that the predominant peaks at 1.4 and 1.8 S were intact monomeric Nvjp-1 with frictional ratios of ~ 2.9 and ~ 1.6 , respectively.

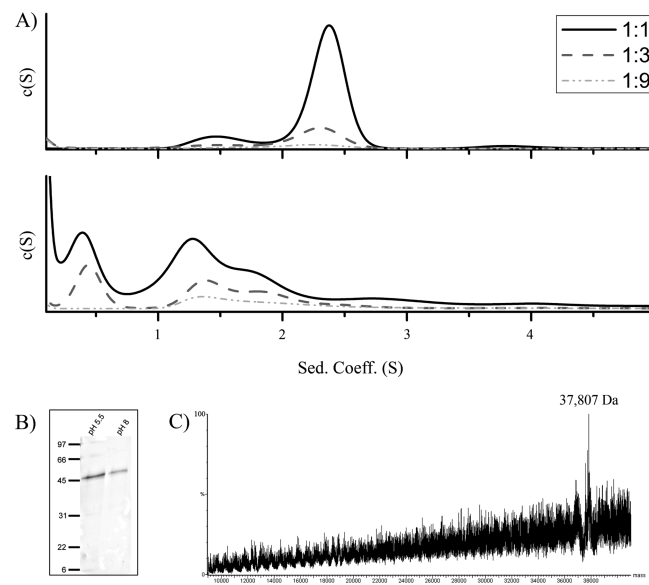


Figure 6. Sedimentation velocity analysis of rNvjp-1. (A) Continuous distributions of rNvjp-1 in 10 mM Tris acetate/100 mM NaCl at pH 5.5 (top) and pH 8 (bottom). (B) Comparison of supernatants of pH adjusted rNvjp-1 by SDS-PAGE. (C) ESI-TOF spectrum of the pH 8 sample in (B).

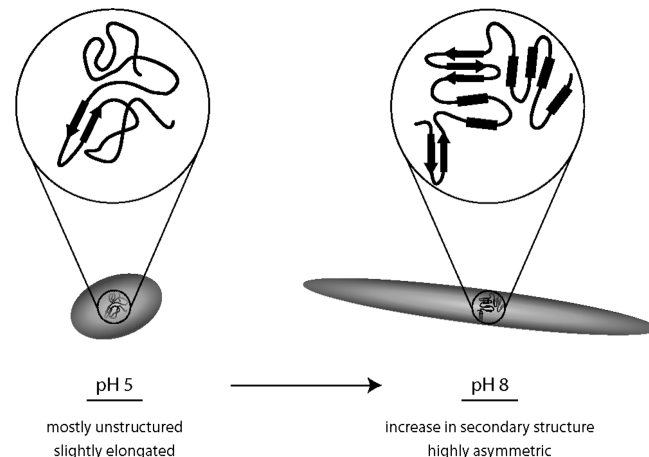


Figure 7. Cartoon depicting the effects of pH on Nvjp-1. Together, data from FTIR and sedimentation velocity analysis suggest that Nvjp-1 undergoes a significant structural and conformation transition in response to pH increase. At pH 5, Nvjp-1 occurs as a slightly elongated monomer comprised mainly of coils and extended turns. Transition to pH 8 results in significant restructuring of Nvjp-1, with the near complete loss of random coil and concomitant increases in α -helix and β -sheet. This structural transition is accompanied by significant elongation of the Nvjp-1 monomer. Fibrillization proceeds following exposure to transition metals.

Discussion

We have described the isolation, molecular cloning, and partial characterization of the histidine-rich protein Nvjp-1 from the jaws of *Nereis virens*. Based on its distribution and abundance, we propose that Nvjp-1 is the primary structural component of the jaw tip. Both acid-urea and SDS-PAGE of jaw extracts indicate that Nvjp-1 is localized throughout the jaw but is enriched in the harder and stiffer distal end. Given the loss of immunoreactivity in structural proteins following sclerotization, the histidine-rich amino acid composition was used to confirm Nvjp-1 content in the sclerotized jaw.^{32–34} Amino acid profiles of both soluble and insoluble fractions from the jaw tip are nearly identical and are comparable to purified

Nvjp-1, although histidine content is somewhat lower in the insoluble material. This discrepancy may be indicative of additional proteins with low histidine content which could offset histidine recovery in insoluble material. Notably, comparison of purified Nvjp-1 and insoluble material from the tip using a Spearman's rank test indicated a strong correlation between the two amino acid compositions ($R_s = 0.9$). Additional proteins are likely to be present in the tip; however, the similarity in overall amino acid composition between soluble and insoluble fractions suggests that their contribution to the structural matrix is relatively low. An alternative explanation is that the protein comprising the insoluble material, although derived from Nvjp-1, may contain more post-translational modifications than that of the extractable fraction. Significant histidine and tyrosine modification has been reported for *Nereis* jaws.¹² Such modifications make accurate histidine quantitation difficult and could themselves hinder protein extraction.

Molecular cloning revealed at least two Nvjp-1 cDNAs, which varied in the presence of two short Gly/His-rich peptide repeats. The difference masses predicted from cDNA of the two variants was similar to the mass difference observed between the major and the minor components in the extract, and Pauly staining confirmed that both components have significant histidine content. An additional truncation variant was also consistently observed (frequency = 0.33, $n = 18$ individual clones), although without additional N-terminal sequence we cannot rule this out as a cloning artifact. Despite extensive screening, including multiple cDNA preparations and 5' RACE strategies, the full N-terminal sequence of Nvjp-1 remains incomplete at this time. Previous reports have described similar difficulties with GC-rich templates.^{35–37} However, given the size of the purified protein and recovered cDNA, only the signal peptide is expected to be missing. As cDNA was generated from pooled worms it is also possible that the variation represents Nvjp-1 polymorphism within the population rather than distinct proteins within an individual. Thus, although there is some evidence for them, the presence of multiple Nvjp-1 variants in the jaw at this point remains hypothetical.

Nvjp-1 joins a growing list of proteins and peptides which form amyloid-like fibers in vitro. Historically, the tendency toward fibrillization was thought to be an exceptional property of proteins, such as α -synuclein, β -amyloid, PrP, and so on, typically associated with the various neurodegenerative amyloidoses (reviewed in ref 38). Recent focus has shifted, however, to diverse proteins for which fiber formation appears to be completely unlinked to disease (reviewed in ref 39). Furthermore, it has been hypothesized that amyloidogenicity may be an inherent property of all polypeptides given appropriate conditions. Aggregates are generally classified as amyloid if they (i) fulfill tinctorial requirements (e.g., bind 'specific' dyes such as thioflavin T or S or exhibit birefringence with Congo Red staining), (ii) have significant cross- β -sheet content, and (iii) exhibit fibrillar morphology.⁴⁰ Nvjp-1 fibers satisfy the final criterion. FTIR data indicate a slight increase in β -sheet content in rNvjp-1 at pH 8. Structural characterization in Zn-induced fibers was not possible due to their insolubility. Corroboration of secondary structure in soluble rNvjp-1 by alternative methods (Raman and CD spectroscopy) was attempted but the results were inconclusive (not shown). Additionally, Zn-induced aggregate exhibited moderate congoophilicity, however, we were unable to resolve fibers from amorphous aggregate (i.e., both were birefringent). Based on these data, rNvjp-1 fibers can be described as "amyloid-like", although further experiments are necessary for definitive classification. Although fibrillization

may not be predictive of function (or dysfunction), there are multiple cases in which a physiological role for amyloid formation has been demonstrated.^{41–47} This is also likely the case for Nvjp-1 as the structural architecture in the jaw strongly suggests that component proteins are fibrous. The dependence of fiber formation on pH and metal coordination is reasonable considering that (i) Nvjp-1 likely experiences a similar pH shift as it progresses from intracellular vesicles (pH < 6) to the extracellular milieu (pH of seawater is ~8) and (ii) Zn ions are readily available in the jaw and associated pulp. It is noteworthy that in vitro fiber formation only occurred at low Zn/protein ratios (≈ 1 and 5), with amorphous aggregate at higher stoichiometries. It is unknown whether assembly in vivo is similarly limited. Even if Nvjp-1 were the sole organic component in the jaw tip, where Zn content can exceed 10% (wt/wt), there would be at least a 60-fold molar excess of Zn to protein. Given additional matrix proteins and halogen content in the tip this value is undoubtedly a gross underestimation of the actual ratio. Nothing is known about fiber assembly in vivo, though it is likely to be tightly regulated given the need for spatial control of protein deposition and to minimize potential toxicity from unrestrained aggregation.

Amyloid formation is believed to occur by a nucleation-dependent mechanism and generally follows significant conversion of secondary structure.^{48–50} Factors such as pH, ionic strength, and metal coordination have been shown to influence fiber formation and morphology.^{24,27,51–55} Based on our data we can reasonably predict that similar features are involved in Nvjp-1 fibrillization. FTIR data suggest that transition from low to high pH is accompanied by the complete loss of random coil and a modest increase in β -sheet, including low frequency bands ($1610–1630\text{ cm}^{-1}$) typically associated with amyloid.³¹ The band observed at 1661 cm^{-1} at low pD has been variably assigned α -helices and extended turns. This band shifts to 1651 cm^{-1} at pD 8. Shifts toward lower frequencies are commonly attributed to increased hydrogen bonding. This suggests that, if the low pD component does represent helices, transition to high pD may lead to helical packing.

Although fiber formation was completely dependent on metal coordination, sedimentation velocity data suggested that Nvjp-1 undergoes a significant change in hydrodynamic properties with transition to high pH in the absence of metals. The predominant component at pH 5.5 (2.3 S) had a calculated frictional ratio (f/f_0) of ~ 1.6 , corresponding to a monomer with an ellipsoid axial ratio of $\sim 8–9$. The sedimentation profile at pH 8 was more complex, with multiple peaks of lower sedimentation coefficients, notably ~ 1.4 and ~ 1.8 S. The reduction in S from 2.3 to 1.4–1.8 suggests that monomer becomes significantly elongated at high pH. This interpretation is supported by direct characterization, notably SDS-PAGE and ESI mass spectrometry, and by modeling of the sedimentation data. Furthermore, this suggests that the rNvjp-1 monomer is able to adopt multiple conformations at pH 8. To appear as distinct species by sedimentation, the different forms must be meta-stable on the order of at least 10s of minutes (i.e., all equilibria are slow).⁵⁶

Conclusions

Nvjp-1 at the jaw tip has radically different mechanical properties from the typical "molten globule" precursors that are stockpiled in the granules of secretory cells. Although specific steps in the cellular processing of Nvjp-1 remain unknown, it is clear from our work that pH, ionic strength, and Zn ions provide effective switches for transforming the soluble precursor

into an asymmetric self-assembling building block. It is probable that similar switches can be designed to trigger synthetic polyimidazoles to form high performance materials.

Acknowledgment. This work was supported by NIH BRP DE014672 and NASA University Research Engineering and Technology Institute (URETI) on Bio-Inspired Materials under Award No. NCC-1-02037.

References and Notes

- Broomell, C. C.; Mattoni, M. A.; Zok, F. W.; Waite, J. H. Critical role of zinc in hardening of *Nereis* jaws. *J. Exp. Biol.* **2006**, *209*, 3219–3225.
- Lichtenegger, H. C.; Schoberl, T.; Bartl, M. H.; Waite, J. H.; Stucky, G. D. High abrasion resistance with sparse mineralization: Copper biomineral in worm jaws. *Science* **2002**, *298*, 389–392.
- Lichtenegger, H. C.; Schoberl, T.; Ruokolainen, J. T.; Cross, J. O.; Heald, S. M.; Birkedal, H.; Waite, J. H.; Stucky, G. D. Zinc and mechanical prowess in the jaws of *Nereis*, a marine worm. *Proc. Natl. Acad. Sci. U.S.A.* **2003**, *100*, 9144–9149.
- Schofield, R. M. S.; Nesson, M. H.; Richardson, K. A. Tooth hardness increases with zinc-content in mandibles of young adult leaf-cutter ants. *Naturwissenschaften* **2002**, *89*, 579–583.
- Moses, D. N.; Harrel, J. H.; Stucky, G. D.; Waite, J. H. Melanin and *Glycera* jaws: Emerging darkside of a robust biocomposite. *J. Biol. Chem.* **2006**, *281*, 34826–34832.
- Vincent, J. F. V.; Wegst, U. G. K. Design and mechanical properties of insect cuticle. *Arthropod Struct. Dev.* **2004**, *33*, 187–199.
- Voss-Foucart, M.; Fonze-Vignaux, M.; Jeuniaux, C. Systematic characters of some polychaetes (Annelida) at the level of the chemical composition of the jaws. *Biochem. Syst.* **1973**, *1*, 119–122.
- Moses, D. N.; Mattoni, M. A.; Slack, N. L.; Waite, J. H.; Zok, F. W. The role of melanin in mechanical properties of *Glycera* jaws. *Acta Biomater.* **2006**, *2*, 521–530.
- Quicke, D. L. J.; Wyeth, P.; Fawke, J. D.; Basibuyuk, H. H.; Vincent, J. F. V. Manganese and zinc in the ovipositors and mandibles of hymenopterous insects. *Zool. J. Linnean Soc.* **1998**, *124*, 387–396.
- Schofield, R. M. S.; Lefevre, H. High-concentrations of zinc in the fangs and manganese in the teeth of spiders. *J. Exp. Biol.* **1989**, *144*, 577–581.
- Broomell, C. C.; Waite, J. H. unpublished results.
- Birkedal, H.; Khan, R.; Slack, N.; Broomell, C. C.; Lichtenegger, H. C.; Zok, F.; Stucky, G. D.; Waite, J. H. Halogenated veneers: Protein cross-linking and halogenation in the jaws of *Nereis*, a marine polychaete worm. *ChemBioChem* **2006**, *7*, 1392–1399.
- Bryan, G. W.; Gibbs, P. E. Zinc—A major inorganic component of nereid jaws. *J. Mar. Biol. Assoc. U. K.* **1979**, *59*, 969–973.
- Waite, J. H.; Benedict, C. V. *Methods Enzymol.* **1984**, *107*, 397–413.
- Ahmad, Z.; Mark, J. E. Biomimetic materials: recent developments in organic-inorganic hybrids. *Mater. Sci. Eng., C* **1998**, *6*, 183–196.
- Laemmli, U. K. Cleavage of structural proteins during assembly of head of Bacteriophage-T4. *Nature* **1970**, *227*, 680–685.
- Paz, M.; Fluekinger, R.; Boak, A.; Kagan, H. M.; Gallop, P. M. Specific detection of quinoproteins by redox-cycling staining. *J. Biol. Chem.* **1991**, *266*, 689–692.
- Sahal, D.; Kannan, R.; Sinha, A.; Babbarwal, V.; Gnana; Prakash, G.; Chauhan, V. S. Specific and instantaneous one-step chemodetection of histidine-rich proteins by Pauly's stain. *Anal. Biochem.* **2002**, *308*, 405–408.
- Sorensen, S. B.; Sorensen, T. L.; Breddam, K. Fragmentation of proteins by *S. aureus* strain V8 protease. *FEBS Lett.* **1991**, *294*, 195–197.
- Waite, J. H. *Anal. Biochem.* **1991**, *192*, 429–433.
- Byler, D. M.; Susi, H. Examination of the secondary structure of proteins by deconvolved FTIR spectra. *Biopolymers* **1986**, *25*, 469–487.
- Brown, P. H.; Schuck, P. Macromolecular size-and-shape distributions by sedimentation velocity analytical ultracentrifugation. *Biophys. J.* **2006**, *90*, 4651–4661.
- Schuck, P. Size-distribution analysis of macromolecules by sedimentation velocity ultracentrifugation and Lamm equation modeling. *Biophys. J.* **2000**, *78*, 1606–1619.
- Fraser, P. E.; Nguyen, J. T.; Surewicz, W. K.; Kirschner, D. A. pH-Dependent structural transitions of Alzheimer amyloid peptides. *Biophys. J.* **1991**, *60*, 1190–1201.
- Narayanan, S.; Reif, B. Characterization of chemical exchange between soluble and aggregated states of β -amyloid by solution-state NMR upon variation of salt conditions. *Biochemistry* **2005**, *44*, 1444–1452.
- Richelli, F.; Buggio, R.; Drago, D.; Salmona, M.; Forloni, G.; Negro, A.; Tognon, G.; Zatta, P. Aggregation/fibrillogenesis of recombinant human prion protein and Gerstmann–Straussler–Sheinker disease peptides in the presence of metal ions. *Biochemistry* **2006**, *45*, 6724–6732.
- Fujiwara, S.; Matsumoto, F.; Yonezawa, Y. Effects of salt concentration on association of the amyloid protofilaments of hen egg white lysozyme studied by time-resolved neutron scattering. *J. Mol. Biol.* **2003**, *331*, 21.
- Goormaghtigh, E.; Cabiaux, V.; Ruysschaert, J. M. Secondary structure and dosage of soluble and membrane proteins by attenuated total reflection Fourier-transform infrared spectroscopy on hydrated films. *Eur. J. Biochem.* **1990**, *193*, 409–420.
- Serrano, V.; Liu, W.; Franzen, S. An infrared spectroscopic study of the conformational transition of elastin-like peptides. *Biophys. J.* **2007**, *93*, 2429–2435.
- Torrent, J.; Alvarez-Martinez, M. T.; Harricane, M. C.; Heitz, F.; Lautard, J. P.; Balny, C.; Lange, R. High pressure induces scrapie-like prion protein misfolding and amyloid fibril formation. *Biochemistry* **2004**, *43*, 7162–7170.
- Zurdo, J.; Guijarro, J. I.; Dobson, C. M. Preparation and characterization of purified amyloid fibrils. *J. Am. Chem. Soc.* **2001**, *123*, 8141–8142.
- Terwilliger, N. B.; Ryan, M. C.; Towle, D. Evolution of novel functions: Cryptocyanin helps build new exoskeleton in cancer magister. *J. Exp. Biol.* **2005**, *208*, 2467–2474.
- Koch, A. W.; Holstein, T. W.; Mala, C.; Kurz, E.; Engel, J.; David, C. N. Spinalin, a new glycine- and histidine-rich protein in spines of Hydra nematocysts. *J. Cell Sci.* **1998**, *111*, 1545–1554.
- Anderson, K. E.; Waite, J. H. Immunolocalization of Dpfpl, a byssal protein of the zebra mussel *Dreissena polymorpha*. *J. Exp. Biol.* **2000**, *203*, 3065–3076.
- Exposito, J. Y.; Ouazana, R.; Garrone, R. Cloning and sequencing of a Porifera partial cDNA coding for a short-chain collagen. *Eur. J. Biochem.* **1990**, *190*, 401–406.
- Chen, J. H.; Turner, P. C.; Rees, H. H. Molecular cloning and induction of nuclear receptors from insect cell lines. *Insect Biochem. Mol. Biol.* **2002**, *32*, 657–667.
- Hayashi, C. Y.; Lewis, R. L. Evidence from flagilliform silk cDNA for the structural basis of elasticity and modular nature of spider silks. *J. Mol. Biol.* **1998**, *275*, 773–784.
- Chiti, F.; Dobson, C. M. Protein misfolding, functional amyloid, and human disease. *Annu. Rev. Biochem.* **2006**, *75*, 333–366.
- Stefani, M. Protein misfolding and aggregation: New examples in medicine and biology of the dark side of the protein world. *Biochim. Biophys. Acta* **2004**, *1739*, 5–25.
- Faendrich, M. On the structural definition of amyloid fibrils and other polypeptide aggregates. *Cell. Mol. Life Sci.* **2007**, *64*, 2066–2078.
- Chapman, M. R.; Robinson, L. S.; Pinkner, J. S.; Roth, R.; Heuser, J.; Hammar, M.; Normark, S.; Hultgren, S. J. Role of *Escherichia coli* curli operons in directing amyloid fiber formation. *Science* **2002**, *295*, 851–855.
- Claessen, D. R.; de Jong, W.; Siebring, J.; de Vreugd, P.; Boersma, F. G.; Dijkhuizen, L.; Wosten, H. A. A novel class of secreted hydrophobic proteins is involved in aerial hyphae formation in *Streptomyces coelicolor* by forming amyloid-like fibrils. *Genes Dev.* **2003**, *17*, 1714–1726.
- Eaglestone, S. S.; Cox, B. S.; Tuite, M. F. Translation termination efficiency can be regulated in *Saccharomyces cerevisiae* by environmental stress through a prion-mediated mechanism. *EMBO J.* **1999**, *18*, 1974–1981.
- Iconomidou, V. A.; Vriend, G.; Hamodrakas, S. J. Amyloids protect the silkworm oocyte and embryo. *FEBS Lett.* **2000**, *479*, 141–145.
- Mackay, J. P.; Matthews, J. M.; Winefield, R. D.; Mackay, L. G.; Haverkamp, R. G.; Templeton, M. D. The hydrophobin EAS is largely unstructured in solution and functions by forming amyloid-like structures. *Structure* **2001**, *9*, 83–91.
- Si, K.; Lindquist, S.; Kandel, E. R. A neuronal isoform of the aplysia CPEB has prion-like properties. *Cell* **2003**, *115*, 879–891.
- True, H. L.; Lindquist, S. L. A yeast prion provides a mechanism for genetic variation and phenotypic diversity. *Nature* **2000**, *407*, 477–483.
- Powers, E. T.; Powers, D. L. The kinetics of nucleated polymerizations at high concentrations: Amyloid fibril formation near and above the supercritical concentration. *Biophys. J.* **2006**, *91*, 122–132.

- (49) Ruschak, A. M.; Miranker, A. D. Fiber-dependent amyloid formation as catalysis of an existing reaction pathway. *Proc. Natl. Acad. Sci. U.S.A.* **2007**, *104*, 12341–12346.
- (50) Pan, K. M.; Baldwin, M.; Nguyen, J.; Gasset, M.; Serban, A.; Groth, D.; Mehlhorn, I.; Huang, Z.; Fletterick, R. J.; Cohen, F. E.; Prusiner, S. B. Conversion of α -helices into β -sheets features in the formation of the scrapie prion protein. *Proc. Natl. Acad. Sci. U.S.A.* **1993**, *90*, 10962–10966.
- (51) Dong, J. J.; Shokes, J. E.; Scott, R. A.; Lynn, D. G. Modulating amyloid self-assembly and fibril morphology with Zn(II). *J. Am. Chem. Soc.* **2006**, *128*, 3540–3542.
- (52) Jobling, M. F.; Huang, X.; Stewart, L. R.; Barnham, K. J.; Curtain, C.; Volitakis, I.; Perugnini, M.; White, A. R.; Cherny, R. A.; Masters, C. L.; Barrow, C. J.; Collins, S. J.; Bush, A. I.; Cappai, R. Copper and zinc binding modulates the aggregation and neurotoxic properties of the prion peptide PrP106–126. *Biochemistry* **2001**, *40*, 8073–8084.
- (53) Bush, A. I.; Pettingell, W. H.; Multhaup, G. D.; Paradis, M.; Vonsattel, J. P.; Gusella, J. F.; Beyreuther, K.; Masters, C. L.; Tanzi, R. E. Rapid induction of Alzheimer A β -amyloid formation by zinc. *Science* **1994**, *265*, 1464–1467.
- (54) Jones, C. E.; Abdelraheim, S. R.; Brown, D. R.; Viles, J. H. Preferential Cu(II) coordination by His96 and His111 induces β -sheet formation in the unstructured amyloidogenic region of the prion protein. *J. Biol. Chem.* **2004**, *279*, 32018–32027.
- (55) Nichols, M. R.; Moss, M. A.; Reed, D. K.; Lin, W. L.; Mukhopadhyay, R.; Hoh, J. H.; Rosenberry, T. L. Growth of β -amyloid(1–40) protofibrils by monomer elongation and lateral association. Characterization of distinct products by light scattering and atomic force microscopy. *Biochemistry* **2002**, *41*, 6115–6127.
- (56) Stafford, W. F.; Sherwood, P. J. Analysis of heterologous interacting systems by sedimentation velocity: Curve fitting algorithms for estimation of sedimentation coefficients, equilibrium and kinetic constants. *Biophys. Chem.* **2004**, *108*, 231–243.

BM800200A